Applied Ocean Research 173 (2026) 105141

Contents lists available at ScienceDirect

Applied Ocean Research

journal homepage: www.elsevier.com/locate/apor

Research paper

Influence of dynamic modeling approaches on the hydrodynamic pressure regeneration on floating structures

Jian Tan [a],*, George Lavidas [a], Harry Bradford Bingham [b]

[a] Faculty of Civil Engineering and Geosciences, Delft University of Technology, Stevinweg 1, 2628 CN, Delft, The Netherlands
[b] Department of Civil and Mechanical Engineering, Technical University of Denmark, Kgs. Lyngby, Denmark

ARTICLE INFO

Keywords:
Pressure regeneration
Linearization techniques
Floating structures
Global dynamic responses

ABSTRACT

Obtaining the hydrodynamic pressure distribution on the wetted surface of floating structures is a critical step in structural analysis and is commonly achieved through pressure regeneration based on predicted global dynamic responses. Using derived hydrodynamic coefficients, various dynamic modeling approaches, including Cummins-equation-based nonlinear time-domain modeling, statistical linearization, and Lorentz linearization, can be applied to solve for the global dynamics of structures subjected to specific wave conditions. These dynamic modeling approaches differ in both computational efficiency and modeling fidelity. Despite their widespread use, a systematic comparison of these approaches, particularly between statistical and Lorentz linearization in predicting global dynamics and regenerated pressure fields, remains limited. This study addresses this gap by conducting a comparative study of linear-potential-flow-based dynamic modeling approaches using a generic cylindrical floater, incorporating a representative nonlinear external machinery effect through different modeling approaches. The resulting global responses are used to regenerate hydrodynamic pressure distributions, showing that all the dynamic modeling approaches agree well under low wave steepness. As wave steepness increases, the prediction performance of statistical linearization, Lorentz linearization, and a simplified Lorentz linearization, gradually decreases relative to the nonlinear time-domain model. Among these, the statistical linearization approach provides results closer to the nonlinear time-domain model than both Lorentz-based linearization methods, particularly in capturing global dynamics and reconstructing hydrodynamic pressure distributions under relatively high wave steepness. Given its high computational efficiency, the statistical linearization approach has the potential to be further developed as an efficient alternative modeling for estimating dynamic responses and hydrodynamic pressure distributions.

1. Introduction

The offshore floating renewable energy sector has gained increasing attention in recent years due to its substantial potential to contribute to the green energy transition. Floating offshore renewable energy systems include floating offshore wind turbines (FOWTs), wave energy converters (WECs), and floating photovoltaic platforms (Magagna and Uihlein, 2015; Martínez et al., 2023). However, the complexity of the offshore environment poses significant challenges for the design of these systems, particularly with regard to their floating structures. To ensure both robustness and cost-effectiveness, it is essential to comprehensively analyze the structural loads experienced by floating designs under a wide range of ocean wave conditions.

Generally speaking, the structural load assessment of floating structures can be carried out using two main approaches. The first is experimental wave-tank testing, which has long been employed to measure stresses or bending moments by placing load cells at critical locations on scaled floating models (Chakrabarti, 1998). However, the high economic and time costs associated with wave-tank experiments make them feasible primarily for final-stage design evaluations. The second main approach is numerical simulation. The integration of hydrodynamic modeling and the finite element method (FEM) has been widely adopted to facilitate the structural design of floating systems. Specifically, hydrodynamic modeling is used to estimate the hydrodynamic and hydrostatic loads exerted on the floaters, which are subsequently applied as input to FEM for detailed structural analysis (Gao et al., 2023). Numerical modeling approaches are more suitable for early- or middle-stage design and optimization of offshore floating structures.

Applying hydrodynamic modeling to obtain the pressure distribution on the wetted hull is an important step in the structural analysis

* Corresponding author.
E-mail address: j.tan-2@tudelft.nl (J. Tan).

https://doi.org/10.1016/j.apor.2026.105141
Received 24 March 2026; Received in revised form 13 May 2026; Accepted 10 June 2026
Available online 21 June 2026

of floating structures. Various modeling approaches exist for capturing the distributed hydrodynamic loads on these systems. Computational fluid dynamics (CFD), a fully nonlinear approach that numerically solves the Navier–Stokes equations, can inherently produce the instantaneous pressure field across the entire computational domain Huo et al. (2024). However, the substantial computational cost of CFD hinders its extensive application in the preliminary design phase where numerous simulations of one to three hours are typically required to adequately represent the stochastic nature of the ocean environment and estimate power performance and structural loading (Kvittem and Moan, 2015). Consequently, more computationally efficient numerical modeling approaches are often preferred in practical applications, and some representative efficient approaches are reviewed below.

As an empirical equation, the Morison formula has been widely used in the design of offshore floating structures. Based on the rigid body assumption in global analysis, the dynamic motions of the floater can be derived for different environmental inputs. Using these dynamic responses, the instantaneous hydrodynamic loads on individual wetted panels can then be approximated with the Morison formula by treating the floater as a slender structure. This enables the estimation of cross-sectional loads on structural components (Gao et al., 2023). The method has been employed for decades in floating structure analysis because of its relatively low computational cost and straightforward implementation (Robertson et al., 2013). For example, the University of Tokyo has developed an in-house code, NK-UTWind, to analyze the coupled dynamics and load effects of FOWTs (Suzuki et al., 2020). In NK-UTWind, hydrodynamic loads are calculated using the Morison formula, and the modeling accuracy has been validated experimentally for FOWTs composed of submerged slender elements. However, the Morison formula cannot be used for non-slender floating structures where radiation/diffraction effects are important (Luan et al., 2017).

Another efficient numerical approach for constructing distributed hydrodynamic and hydrostatic pressure fields is based on linear radiation–diffraction theory using the boundary element method (BEM), which is widely applied in offshore engineering (Robertson et al., 2013). In this approach, frequency-dependent hydrodynamic coefficients of integrated forces and moments on the rigid floater and a set of frequency-dependent hydrodynamic pressure coefficients at specified points on the floater are initially derived via BEM. Then, by applying either a time-domain (TD) dynamic model based on the Cummins equation (Cummins et al., 1962) or a linear frequency-domain (FD) dynamic model based on harmonic analysis (Tan et al., 2025a), the global dynamic responses of the floater can be obtained for specified environmental conditions. For TD modeling, an intermediate step is to transform the motion responses into the time domain using an inverse fast Fourier transform (IFFT). Once the time-dependent motions are available, the instantaneous hydrodynamic pressure distribution on the hull can be reconstructed by combining the motion responses with the precomputed pressure coefficients. This approach has gained significant research interest in recent years because it provides a good balance between modeling accuracy and computational efficiency. For instance, a representative commercial software, namely WADAM developed by Det Norske Veritas (DNV), enables the computation of dynamic responses of floating structures by a linear FD modeling approach (DNV, 2019). Subsequently, hydrodynamic pressure mapping on the hull can be constructed by the software for deeper structural analysis through FEM. In Gao et al. (2023), a methodology was proposed to assess the floater stress of FOWTs, incorporating both wind- and wave-induced loads. The global motion of the FOWT was first obtained using a TD dynamic model, and the corresponding hydrodynamic pressure distribution on the hull was regenerated as input to a structural analysis model. Similarly, in Wang et al. (2023), structural loading on a semi-submersible 10-MW FOWT were investigated using a new modeling framework primarily based on the DNV SESAM package. Hydrodynamic and hydrostatic pressures were recalculated from the global motions derived by a nonlinear Cummins-equation TD model implemented in the SESAM SIMA module, and then applied in a structural model built in GeniE. By verification against a reference FD approach, it suggested that the established modeling framework associated with hydrodynamic/hydrostatic pressure recalculation could effectively facilitate the analysis of global and internal loads of the semi-submersible floater. The above-mentioned studies have not only demonstrated the established methodologies for determining hydrodynamic pressure distributions on floating structures but also underlined the significance of hydrodynamic pressure reconstruction in in-depth structural analysis.

As discussed above, regenerating the pressure distribution on the hull using radiation-diffraction theory relies on the accurate prediction of the global dynamic motion responses of the floating structure. BEM solvers based on linear potential-flow theory have been widely used to address wave-structure interaction problems due to their high computational efficiency. They provide solutions in the form of frequency-dependent hydrodynamic coefficients, which can then be used to derive global motion responses through different types of dynamic modeling approaches for different environmental conditions. Predominately-used dynamic modeling approaches include linear FD modeling and nonlinear Cummins-equation-based TD modeling and FD modeling with linearization approaches. The commonly-applied linearization approaches in offshore engineering are represented by statistical linearization (SL) method and Lorentz linearization method, in which Lorentz linearization is particularly used to address quadratic damping terms (Terra et al., 2005). These dynamic modeling approaches differ in modeling fidelity and computational demand; thus, they have coexisted for a long period in offshore engineering and are widely applied for different purposes or design stages (Karimirad, 2014; Jonkman, 2009; 201, 2016). For instance, in Tan et al. (2025a, 2022a), Silva et al. (2020), linear FD modeling, nonlinear TD modeling, and SL approaches were applied to predict various performance indicators of a floating point-absorber wave energy converter. Some typical nonlinear effects were addressed in these studies, comprising viscous drag forces, nonlinear external machinery damping forces and nonlinear spring effects. Their results indicated that neglecting nonlinearities in linear FD modeling leads to a noticeable overestimation in fatigue loads and power absorption under energetic sea states, whereas the SL approach yielded results comparable to the nonlinear TD model. In other studies (Kluger et al., 2016; Silva et al., 2021; Hall, 2013; Abdelmoteleb and Bachynski-Polić, 2025), SL techniques were used to incorporate nonlinear effects on FOWTs within an FD framework, demonstrating high computational efficiency together with improved accuracy in predicting global dynamic responses relative to linear FD modeling. In Tom et al. (2016), Al Shami et al. (2019), Xu et al. (2019), Lorentz linearization was used to include the viscous drag effect in the FD modeling approach for analyzing the global dynamics of floating structures, suggesting an improved prediction performance compared to the linear FD modeling approach. Even though these studies have demonstrated the applicability of those dynamic modeling approaches in prediction of global dynamics and global loads of floating structures, their prediction performance has not been comprehensively compared, particularly considering different linearization methods. Further, it still remains largely unexplored to what extent the selected dynamic modeling approach propagates the modeling uncertainty in global dynamic analysis to hydrodynamic pressure regeneration.

The present article aims to investigate the influence of the selection of dynamic modeling approaches in the prediction of global dynamic responses and further pressure field regeneration of floating structures. The concerned dynamic modeling approaches include nonlinear TD modeling, SL, Lorentz linearization, and a simplified Lorentz linearization. A typical nonlinear effect, representing external machinery forces, relevant to the dynamics of offshore floating structures is discussed in this study. A generic heaving floating cylinder is considered as the research object. The dynamic motion responses estimated by the four global dynamic modeling approaches are applied as input to

Table 1
Simulation parameters of the cylindrical floater.

Parameters	Quantities
Cylinder radius:	5 m
Cylinder height:	10 m
Cylinder mass: M_{cy}	402520 kg
Projected area: A_s	78.5 m^2
Floater draft:	5 m
Water depth:	100 m
Water density: ρ	1025 kg/m^3
Mooring line tension in heave: $K_{mooring}$	20 kN/m
Damping coefficient of external force: R_{ext}	600 kNs/m

reconstruct the pressure distributions on the hull. To construct the pressure field, the frequency-dependent pressure coefficients of the floater at each panel are derived using the open-source BEM solver NEMOH (Penalba et al., 2017b). The instantaneous pressure results regenerated based on the dynamic responses predicted by the different dynamic modeling approaches are compared across different sea states. Additionally, pressure profiles at specific locations on the hull are evaluated. The discrepancies between the pressure results obtained based on SL and Lorentz linearization approaches relative to the nonlinear TD modeling are demonstrated.

2. Methodology

2.1. Floater description

Floating structures are commonly employed as a component to support offshore operations, such as FWOTs and WECs. A generic cylindrical floater is considered in this work to represent offshore floating structures, as illustrated in Fig. 1. The floater is constrained to oscillate only in heave mode. The mooring tensions are modeled as linear spring force. More relevant simulation parameters of the floater are specified in Table 1.

The cylindrical floater considered in this study is intended to represent a generic representative of offshore floating structures, such as the column element of FOWTs or a heaving-type WEC. The geometric and physical parameters are selected to constitute a physically consistent and representative test case of realistic offshore scale. The mooring stiffness provides a light linear restoring force in heave, and the external damping coefficient is chosen to introduce a moderate but observable level of nonlinear loading, sufficient to clearly differentiate the performance of the four modeling approaches across the three sea states without causing severe dynamic conditions.

2.2. Global dynamic modeling

Global dynamic motion responses of the floating structure will be used as input to reconstruct the pressure distribution on the hull. For comparison, different global dynamic modeling approaches are applied in this work to estimate global dynamic motion responses. The formulation of these dynamic modeling approaches are presented in the following text.

2.3. Representation of irregular waves

Before getting into the formulation of the dynamic modeling approaches, a brief introduction of the representation of ocean waves is provided. In Airy wave theory, irregular waves can be described by the summation of a range of regular wave components with random phases. Then, the wave elevation of a unidirectional irregular wave train is expressed as

$$\eta_{irr}(x,t) = \sum_{j=1}^{N} A_j(\omega_j)\cos\left(k_j x - \omega_j t - \phi_j\right) \tag{1}$$

where k_j, A_j and ϕ_j are the wave number, wave amplitude and phase angle corresponding to the regular wave component of angular frequency ω_j. To represent irregular wave conditions, the wave spectrum is discretized into frequency bins of width $\Delta\omega$, and the wave amplitude at the frequency component ω_j is given as

$$A_j(\omega_j) = \sqrt{2\,S(\omega_j)\Delta\omega} \tag{2}$$

where $S(\omega_j)$ is power spectral density corresponding to the frequency ω_j.

2.3.1. Nonlinear time-domain modeling

The motion of floating structures in the time domain is commonly described by the Cummins equation (Cummins et al., 1962):

$$[M + M_r(\infty)]\ddot{z}(t) = F_e(t) + F_{mooring}(t) + F_{ext}(t) + F_{hs}(t) - \int_{-\infty}^{t} K_{rad}(t-\tau)\dot{z}(\tau)d\tau \tag{3}$$

where

M: mass of the floating structure;
$M_r(\infty)$: added mass at infinite frequency;
z, $\dot{z}$, $\ddot{z}$: displacement, velocity, and acceleration of the floater;
t: time;
F_e: wave excitation force, and $F_e(t) = \sum_{j=1}^{N} A_j(\omega_j)\hat{f}_e(\omega_j)\cos\left(\omega_j t - \phi_j\right)$, in which $\hat{f}_e$ is the excitation force coefficient;
$F_{mooring}$: linear mooring force;
F_{hs}: hydrostatic force;
F_{ext}: nonlinear external machinery force;
K_{rad}: radiation impulse function;
τ: intermediate variable in the convolution integral.

The term F_{ext} is applied here to exemplify external nonlinear machinery forces. As the floater dynamics are evaluated deterministically at each time step, the nonlinear term F_{ext} can be included directly in the TD model, as

$$F_{ext}(t) = -R_{ext}\dot{z}(t)|\dot{z}(t)| \tag{4}$$

where R_{ext} is the damping coefficient of the external machinery force, and its value is defined as 600 kN/m in this case.

2.3.2. Statistical linearization approach

The SL approach can be regarded as an extension of the linear FD modeling method, while nonlinear effects can be incorporated by additional linear equivalent terms. The fundamental principle of the SL technique is to find a linear equivalent term which is expected to dissipate the same amount of energy as the exact nonlinear term in a stationary stochastic process (Roberts and Spanos, 2003). The derivation of the linear equivalent coefficient is given in detail in the Appendix. The equation of motion in the SL approach is expressed as

$$\hat{F}_e(\omega_j) = \hat{z}(\omega_j)\left\{-\omega_j^2\left[M + M_r(\omega_j)\right] + K_{hs} + K_{mooring} + \mathrm{i}\omega_j\left[R_r(\omega_j) + R_{SL,ext}\right]\right\} \tag{5}$$

where

$\hat{F}_e$: complex amplitude of excitation force, and $\hat{F}_e(\omega_j) = A_j(\omega_j)e^{-\mathrm{i}\phi_j}\hat{f}_e(\omega_j)$;
ω_j: angular frequency corresponding to j_{th} component;
$\hat{z}$: complex amplitude of displacement;
$K_{mooring}$: mooring stiffness coefficient;
K_{hs}: hydrostatic stiffness coefficient;
R_r: radiation damping coefficient;
$R_{SL,ext}$: equivalent linearized external damping coefficient.

It is noted that $R_{SL,ext}$ is frequency-independent and related to statistical estimates of the system responses. An iterative algorithm is applied to solve (5) since the linearized coefficients are unknown prior to the solution of the responses.

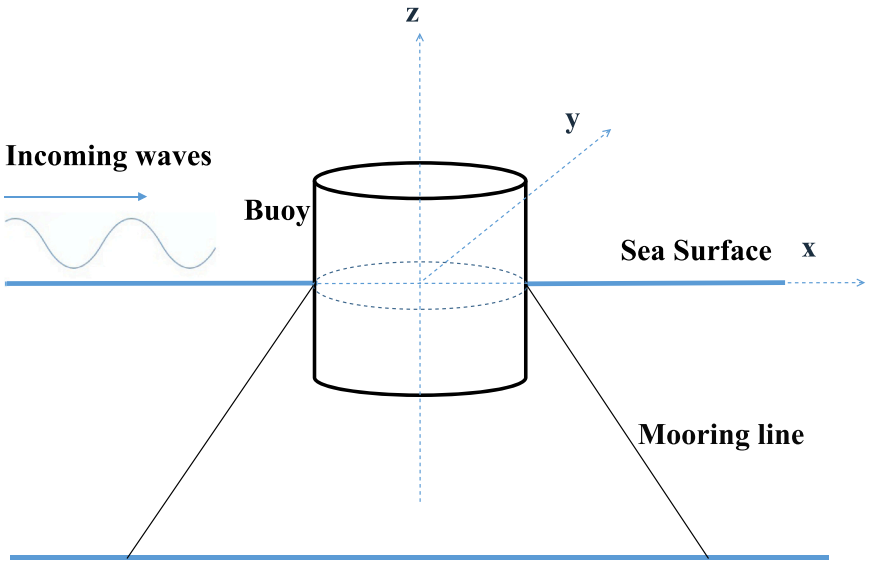

Fig. 1. Schematic of the cylindrical floater.

2.3.3. Lorentz linearization approach

Lorentz linearization is another linearization method to incorporate nonlinear terms into the FD modeling. Different from the SL approach derived assuming a stochastic process of the dynamic system, the Lorentz linearization is intended to find an equivalent linear damping that dissipates the same amount of energy as the nonlinear term within one specific oscillation period (Terra et al., 2005). As demonstrated in previous studies (Folley and Whittaker, 2010), the linearized quadratic damping coefficient derived by the Lorentz linearization method is given as

$$R_{LO,ext}(\omega) = \frac{8}{3\pi} R_{ext} |\hat{z}(\omega)| \omega \tag{6}$$

where $R_{LO,ext}(\omega)$ represents the equivalent linear damping obtained using the Lorentz linearization approach. It is seen in (6) that the linearized damping depends on both the motion amplitude $|\hat{z}(\omega)|$ and the angular frequency ω. Consequently, it can be inferred that the linearized term is directly related to the wave steepness at each frequency component associated with a given wave spectrum. The wave steepness of a specific frequency component can be expressed as

$$\epsilon(\omega) = \frac{2\, A_{lo}(\omega)}{\lambda(\omega)} \tag{7}$$

where A_{lo} represents the localized wave amplitude in the wave spectrum and λ is the wavelength that can be calculated via the dispersion relation. The localized wave amplitude A_{lo} can be derived as

$$A_{lo}(\omega_j) = \sqrt{\int_0^\infty 2\, S(\omega')\, \delta(\omega' - \omega_j)\, \mathrm{d}\omega'} = \sqrt{2\, S(\omega_j)} \tag{8}$$

where $\delta(\cdot)$ denotes the Dirac delta function and $S(\omega_j)$ is the spectral density.

For a given wave spectrum, the equation of motion is applied first for each frequency component to obtain the linearized coefficient, as

$$A_{lo}(\omega_j) e^{-\mathrm{i}\phi_j} \hat{f}_e(\omega_j) = \hat{z}_{lo}(\omega_j) \left\{ -\omega_j^2 \left[M + M_r(\omega_j) \right] + K_{hs} + K_{mooring} + \mathrm{i}\omega_j \left[R_r(\omega_j) + R_{LO,ext}(\omega_j) \right] \right\} \tag{9}$$

where $\hat{z}_{lo}$ represents the complex amplitude of the floater's displacement corresponding to the localized wave amplitude A_{lo}. An iterative scheme is also needed to solve (9), since $R_{LO,ext}$ depends on the displacement amplitude. After $R_{LO,ext}$ is determined for each frequency component, the complex amplitude of the floater's displacement corresponding to ω_j and A_j can be obtained as

$$\hat{z}(\omega_j) = \frac{\hat{z}_{lo}(\omega_j)}{A_{lo}(\omega_j)} A_j(\omega_j) \tag{10}$$

2.3.4. Simplified Lorentz linearization approach

For irregular sea states, Lorentz linearization can also be implemented in a simplified way by using the equivalent damping derived at the peak frequency of the wave spectrum for the entire range of frequency components. In this sense, the equation of motion is first applied for the peak frequency to derive the equivalent damping coefficient, as

$$A_{lo}(\omega_p) e^{-\mathrm{i}\phi_j} \hat{f}_e(\omega_p) = \hat{z}_{lo}(\omega_p) \left\{ -\omega_p^2 \left[M + M_r(\omega_p) \right] + K_{hs} + K_{mooring} + \mathrm{i}\omega_p \left[R_r(\omega_p) + R_{LO,ext}(\omega_p) \right] \right\} \tag{11}$$

where ω_p indicates the peak frequency of the given spectrum. An iterative scheme is also needed to solve the equation.

Subsequently, the derived $R_{LO,ext}(\omega_p)$ is used to derive the dynamic responses at other frequency components, as

$$\hat{F}_e(\omega_j) = \hat{z}(\omega_j) \left\{ -\omega_j^2 \left[M + M_r(\omega_j) \right] + K_{hs} + K_{mooring} + \mathrm{i}\omega_j \left[R_r(\omega_j) + R_{LO,ext}(\omega_p) \right] \right\} \tag{12}$$

2.3.5. Implementation of numerical modeling

Linear Airy wave theory is considered throughout this study. The applied irregular wave train is constructed based on JONSWAP spectrum with a peakedness factor of 3.3. The irregular waves are constructed using a linear superposition of 1000 harmonic wave components. Angular frequencies of these components are distributed between 0.2 and π rad/s, and each component is associated with a random phase shift. Additionally, it should be noted that the modeling approaches described here are inherently available to other types of wave spectrum and parameter choices (Journée et al., 2015).

A consistent set of hydrodynamic coefficients for the cylindrical floater, $M_r(\omega)$, $R_r(\omega)$, and $\hat{f}_e(\omega)$, is employed across the FD modeling, TD modeling and the SL approach. Besides, the frequency-dependent pressure coefficients, including diffraction pressure and radiation pressure at each panel, are also needed to reconstruct the time-dependent pressure distribution on the hull. These coefficients are all obtained using the open-source BEM solver NEMOH (Penalba et al., 2017a) in this

study. In the TD modeling, the convolution term in (3) is approximated by a state-space representation derived via the frequency-domain identification method detailed in Pérez and Fossen (2008), with an aim to reduce computational cost. The equations of motion in the TD modeling are solved using the ODE45 solver in Matlab with zero initial displacement and velocity. To avoid strong initial transient energy flow to the system, a ramp function is adopted during the first 100 s (Lawson et al., 2014), which is excluded from the analysis. The TD modeling framework applied in this work has been validated in previous studies (Tan et al., 2022b, 2023b,a).

The SL, Lorentz linearization and simplified Lorentz linearization approaches are built upon the framework of the FD modeling while an iterative scheme is needed to solve the global dynamic response. A convergence tolerance of 0.1% is defined for the iteration in this work, which is thought sufficiently strict given the purpose of the study (Silva et al., 2020; Folley and Whittaker, 2013). The initial estimate of the displacement's standard deviation is taken from the linear FD modeling results. Convergence criteria is satisfied for all the simulation cases presented in this work.

2.4. Pressure regeneration

The hydrodynamic and hydrostatic pressure distributions on the hull are regenerated based on the predicted global dynamic motion responses of the floater. Different pressure components are recalculated separately, following the method given below. In the linearized boundary conditions of potential flow theory, the dynamic Froude–Krylov pressure and diffraction pressure components are derived using the mean wetted surface. The dynamic Froude–Krylov pressure component at point i (x_i, y_i, z_i) of the hull is thus derived as

$$p_i^{\mathrm{FK}}(t) = \sum_{j=1}^{N} \rho g A_j \, e^{k_j z_i} \cos\left(k_j x_i - \omega_j t - \phi_j\right) \tag{13}$$

where ρ is the water density, g is the gravitational acceleration, A_j is the wave amplitude, k_j is the wave number, ω_j is the wave frequency, and ϕ_j is the wave phase.

The diffraction pressure components at point i (x_i, y_i, z_i) on the hull surface are calculated as

$$p_i^{\mathrm{diff}}(t) = \sum_{j=1}^{N} A_j \, P_{i,j}^{\mathrm{diff}} \cos\left(-\omega_j t - \phi_j + \phi_{i,j}^{\mathrm{diff}}\right) \tag{14}$$

where $P_{i,j}^{\mathrm{diff}}$ and $\phi_{i,j}^{\mathrm{diff}}$ are the diffraction pressure amplitude and phase angle for a particular point i (x_i, y_i, z_i) on the hull at the jth frequency component, calculated by NEMOH.

The hydrostatic pressure and radiation pressure components are regenerated based on the instantaneous dynamic responses of the floater. The hydrostatic pressure at point i can be derived as

$$p_i^{\mathrm{hs}}(t) = -\rho g \left(\boldsymbol{T}\mathbf{Z}[4:6,1](t) + z_i\right) \tag{15}$$

where $\boldsymbol{T}$ stands for a 1×3 transfer matrix that converts the rotation at the defined center of motion to the vertical component at the point i; $\mathbf{Z}$ is the 6×1 displacement matrix of the floater defined with regard to the defined center of motion, in which $\mathbf{Z}[4:6,1]$ corresponds to the response columns for rotation in roll, pitch, and yaw, respectively. Inverse Fast Fourier Transformer (IFFT) is applied to motion results derived by the SL, Lorentz linearization and the simplified Lorentz approaches to obtain the time-dependent motion series $\mathbf{Z}(t)$.

The radiation pressure component at point i can be regenerated as

$$p_i^{\mathrm{rad}}(t) = \sum_{j=1}^{N} \sum_{m=1}^{N_{\mathrm{dof}}} P_{i,m,j}^{\mathrm{rad}} \, |\hat{\mathbf{u}}_j[m,1]| \, \cos\left(-\omega_j t - \phi_{m,j}^{u} + \phi_{i,m,j}^{\mathrm{rad}}\right) \tag{16}$$

where $\hat{\mathbf{u}}$ is the complex amplitude of the velocity matrix of the floater at the frequency component ω_j and $\phi_{m,j}^{u}$ is the corresponding phase angle; $P_{i,m,j}^{\mathrm{rad}}$ and $\phi_{i,m,j}^{\mathrm{rad}}$ are the radiation pressure amplitude and phase angle at point i (x_i, y_i, z_i) on the hull corresponding to the mth degree of freedom (DOF) at the jth frequency component, which are calculated by NEMOH. Fast Fourier Transformer (FFT) is used to convert the time-dependent velocity responses calculated by the nonlinear time-domain model to frequency-dependent form $\hat{\mathbf{u}}$.

The instantaneous total pressure exerted on point i on the hull surface is then obtained by the summation of all the pressure components, as

$$p_i^{\mathrm{total}}(t) = p_i^{\mathrm{FK}}(t) + p_i^{\mathrm{diff}}(t) + p_i^{\mathrm{hs}}(t) + p_i^{\mathrm{rad}}(t) \tag{17}$$

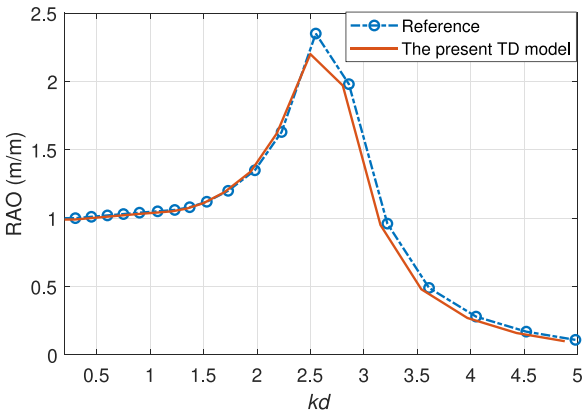

Fig. 2. Comparison bwteen the RAO calculated by the present TD model and verified numerical results published in Shi et al. (2019). k and d stands for the wave number and water depth respectively. (cylinder radius is 4.05 m; cylinder draft is 4.05 m; wave height is 0.5 m; water depth is 15 m.)

Table 2
Simulation cases considered in this study.

Simulation case	T_s	H_s
SC 1 (low wave steepness)	12 s	2 m
SC 2 (medium wave steepness)	12 s	4 m
SC 3 (high wave steepness)	12 s	6 m

3. Results and discussion

3.1. Validation of the nonlinear TD model

As the established nonlinear TD model is considered the 'true' reference, it is essential to validate its accuracy before conducting further investigations. The established TD model is compared against the numerical and experimental results published in Shi et al. (2019), as shown in Figs. 2 and 3. Good agreement is observed between the present TD model and both the numerical and experimental data, suggesting that the present TD model can serve as a reliable reference. It should be noted that the floater used in this validation is not identical to the one applied in the subsequent analysis, as its geometry was modified to match the floater configuration used in the reference study. This modification is considered reasonable for the purpose of validating the implementation and overall structure of the established TD model.

3.2. Global dynamic response prediction

The global dynamic responses predicted by the four dynamic modeling approaches are presented and compared in this section. Three simulation cases (SC 1 - SC 3), characterized by different significant wave heights, are considered to represent sea states ranging from low-to-medium-to-high wave steepness, as summarized in Table 2. The simulation cases SC 1 to SC 3 are ordered to reflect increasing wave steepness.

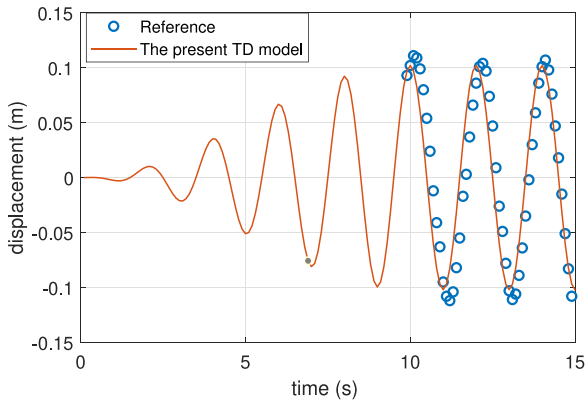

Fig. 3. Comparison between the instantaneous heave displacement derived by the present TD model and experimental results published in Shi et al. (2019). (cylinder radius is 0.4 m; cylinder draft is 0.12 m; wave height is 0.2 m; ; wave period is 2 s; water depth is 1 m.)

The predicted power spectral density (PSD) of the floater displacement is shown in Fig. 4. As illustrated in Fig. 4(a), the four dynamic modeling approaches for SC 1 yield very similar predictions over a wide range of frequency components. As shown in Figs. 4(b) and 4(c), with the increase of the wave steepness, the PSD results predicted by the Lorentz linearization and the simplified Lorentz linearization approaches tend to deviate more from the nonlinear TD modeling approach, particularly in the frequency range between 0.075 and 0.08 Hz. This frequency range corresponds to the peak frequency of the given sea state, and the amplified responses in this region lead to noticeable nonlinear effects. In addition, the simplified Lorentz linearization approach and Lorentz linearization present highly similar PSD value predictions around the peak frequency, while the simplified approach is associated with clearly lower PSD values at high frequencies. This is because the equivalent damping applied in the simplified Lorentz linearization approach is linearized only for the peak frequency, and this equivalent damping is overestimated for other frequencies. This explanation is also supported by the results presented in Fig. 6. Comparatively, the SL method shows only slight deviations from the TD model in the prediction of peak PSD values across all the three sea states considered in this study.

In the SL, Lorentz linearization and simplified Lorentz linearization approaches, the nonlinear quadratic term is represented in different ways in the equations of motion. Specifically, the simplified Lorentz linearization and the SL approach apply a single, consistent equivalent linear damping term across all frequency components for a given sea state, whereas the linearized damping coefficient in the Lorentz linearization method is frequency-dependent. Beyond their influence on the PSD values of the dynamic responses, different handling in linearizing nonlinearities can also lead to discrepancies in the predicted phase shift of the dynamic motion, which also plays an important role in subsequent pressure regeneration. From this perspective, it is necessary to examine the effect of the dynamic modeling approaches on the prediction of phasing.

Fig. 5 presents the phase shift of the floater displacement relative to the excitation force. It can first be observed from the three plots that the prediction performance of the SL, the simplified Lorentz linearization and Lorentz linearization approaches on the phase shifts is frequency dependent. It can be noted that the simplified Lorentz linearization tends to overestimate phase angles and exhibits larger discrepancies than the SL and the Lorentz linearization approaches compared to the nonlinear TD model, across most of the frequency range. Neither the SL nor the Lorentz linearization approach consistently provides superior phase predictions across the entire frequency range. At frequencies above 0.11 Hz, the SL approach yields visibly closer prediction than the nonlinear TD model. Furthermore, in all three plots, the phase shifts predicted by the Lorentz linearization approach tend to deviate noticeably from those of the nonlinear TD model in the frequency band between 0.075 and 0.09 Hz, which corresponds to the peak frequency of the sea states. This observation can be further examined through a comparison of the linear equivalent damping coefficients associated with the different modeling approaches, as illustrated in Fig. 6. Since no explicit linear equivalent damping term is present in the formulation of the nonlinear TD model, an extra step is taken here to find an equivalent damping coefficient for the TD model. This is determined by introducing an additional damping term into the linear FD model such that the displacement amplitude at each frequency matches that obtained from the dynamic response of the TD modeling. To achieve this, FFT is also used to transform the time series of dynamic motion into the frequency domain. Fig. 6 reveals clear differences among the linear equivalent damping coefficients corresponding to the nonlinear TD model, the SL approach, the simplified Lorentz linearization and the Lorentz linearization approach. For the simulation case considered, the simplified Lorentz linearization is associated with the highest equivalent damping coefficient among all the considered four dynamic modeling approaches, and it corresponds to the equivalent damping obtained by the Lorentz linearization approach at the peak frequency. Besides, the Lorentz linearization method exhibits frequency-dependent equivalent damping coefficients, and these coefficients are higher than those obtained from the nonlinear TD model in the frequency range of approximately 0.075–0.09 Hz. This explains the spike in phase shifts predicted by the Lorentz linearization method, as shown in Fig. 5. However, at higher frequencies, the equivalent damping coefficients for the Lorentz linearization approach tend to be noticeably lower than those of the TD model. Comparatively, the equivalent damping coefficients of the SL approach remain consistently higher than those of the TD model across the entire frequency range for the considered simulation case. These differences in linear equivalent damping provide an explanation for the observed deviations in phase shift predictions between the SL, the simplified Lorentz linearization, the Lorentz linearization approaches, and the nonlinear TD modeling approach.

For comparison, the same wave profiles are used in the four different dynamic modeling approaches to obtain the global dynamic responses of the floater for subsequent regeneration of the hydrodynamic pressure on the hull. The wave profiles corresponding to different simulation cases are given in Fig. 7. The global dynamic responses derived by different models for the defined wave profiles are presented in Fig. 8. It can be seen that the time-dependent global responses predicted by the four dynamic modeling approaches appear to be rather close in SC 1 associated with low wave steepness. From SC 2 to SC 3, the discrepancies between these dynamic models start to become more visible, particularly near the peak values of the responses where nonlinear effects are more pronounced. The standard deviation of the global responses predicted by different modeling approaches are depicted in Table 3, showing that all linearized models generally agree well with the TD model under the mild sea state SC 1. Among them, the SL model provides the closest agreement across all cases, with relative errors below 4%, closely followed by Lorentz linearization approach. In contrast, the prediction error of the simplified Lorentz approaches is the largest, and it increases as the wave steepness increases, reaching 18% under SC3.

Computational efficiency is also a crucial factor in the design process of floating structures, especially in the early design stages involving a larger number of design iterations and optimizations. The four dynamic models differ notably in this regard. Their computational times, summarized in Table 4, were obtained using the same Intel i7/2.80 GHz processor to ensure consistency. As shown in Table 4, the simplified Lorentz linearization approach is the most efficient approach, closely followed by the SL approach. Besides, as expected, the Lorentz

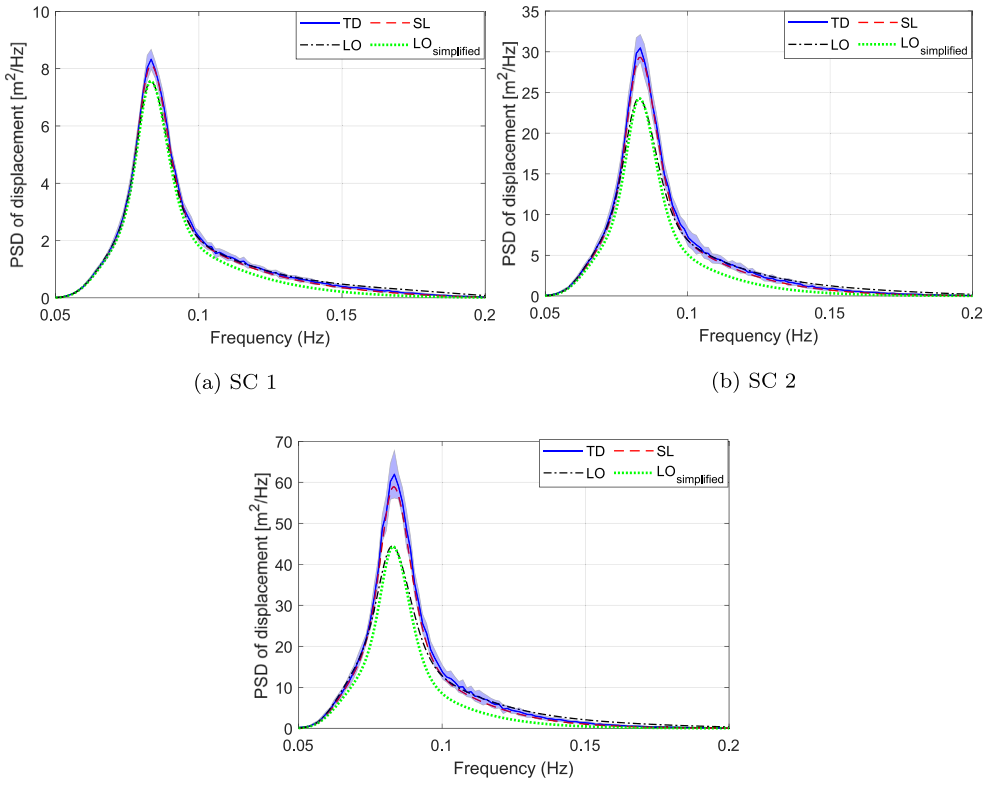

(a) SC 1 (b) SC 2

(c) SC 3

Fig. 4. Prediction comparison of the power spectral density of the floater's displacement in heave motion among different dynamic modeling approaches. The shaded area stands for the standard deviation of multiple realization of TD simulations. 'LO' represents the Lorentz linearization approach, and '$LO_{simplified}$' represents the simplified Lorentz linearization approach.

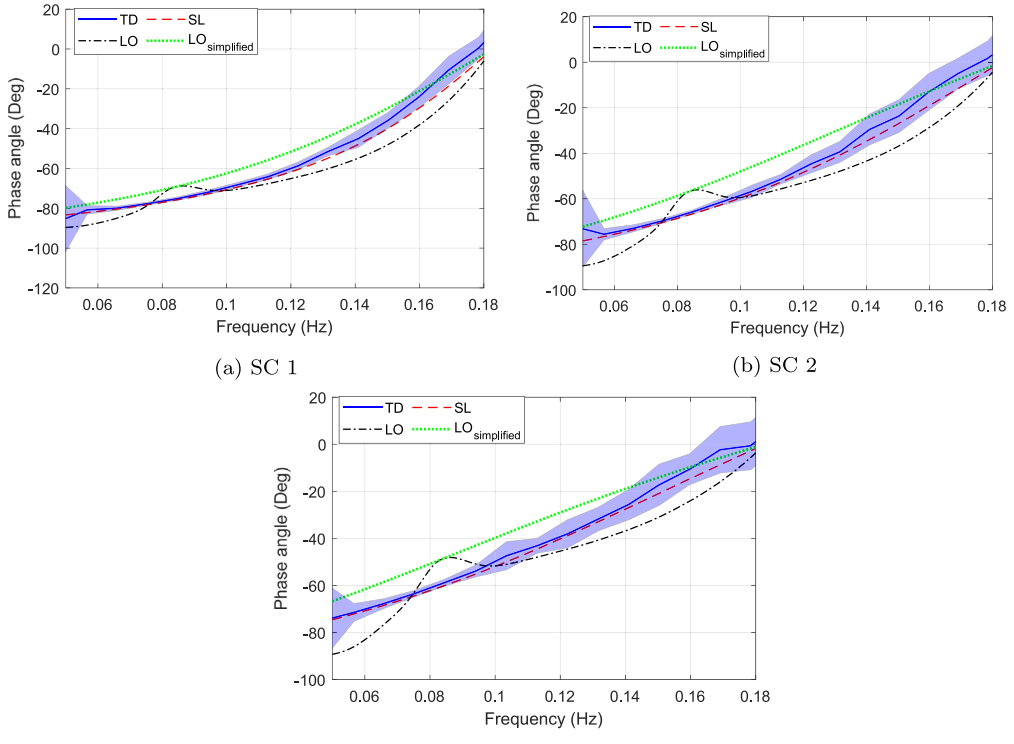

(a) SC 1 (b) SC 2

(c) SC 3

Fig. 5. Prediction comparison of the phase shift of the floater's displacement relative to the excitation force among different dynamic modeling approaches. The shaded area stands for the standard deviation of multiple realization of TD simulations.

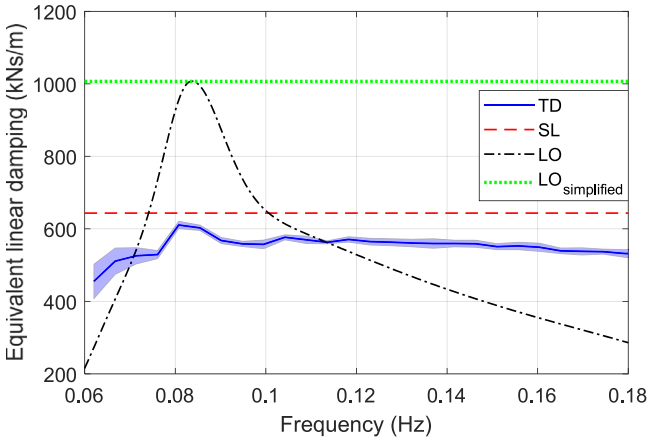

Fig. 6. Comparison of the linear equivalent damping coefficients corresponding to different modeling approaches, and the simulation case is considered as SC 3. The shaded area stands for the standard deviation of multiple realization of TD simulations.

Table 3
Comparison between different dynamic models on the estimation of global displacement of the floater.

Case	Models	STD of displacement (m)	Relative error to TD (%)
SC 1	LO	0.4725	0.90
	$LO_{simplified}$	0.4413	7.45
	SL	0.4718	1.05
	TD	0.4768	–
SC 2	LO	0.8038	2.61
	$LO_{simplified}$	0.7050	14.58
	SL	0.8104	1.81
	TD	0.8253	–
SC 3	LO	1.2026	7.92
	$LO_{simplified}$	1.0711	17.99
	SL	1.2568	3.77
	TD	1.3061	–

linearization approach takes more computational time than the SL approach. This is because the solution for the linear equivalent damping coefficients in the Lorentz Linearization requires iterations for each frequency component. In contrast, the TD model implemented based on ODE 45 solver in Matlab is considerably more expensive. One single run of the TD simulation takes over around 700 and 300 times longer than the SL and the Lorentz linearization approaches, respectively. Moreover, it should be noted that multiple realizations of TD simulations are normally required in practice for achieving statistical results given the random nature of ocean waves, which implies much higher computational loads of the TD model.

3.3. Hydrodynamic pressure regeneration

The regenerated hydrostatic and hydrodynamic pressure results are presented in this subsection. To facilitate visualization, an x-y cross-section of the floater hull is selected as the examined curve, located 4 m below the still water level, as illustrated in Fig. 9. The total pressure distributions along the examined curve at several representative time instants are shown in Figs. 10–12.

As shown in Fig. 10, corresponding to SC 1, the differences among the four models are relatively small, and the pressure variation trends along the curve predicted by the simplified Lorentz linearization, the Lorentz linearization approach, and the SL approach are in good agreement with those obtained from the nonlinear TD model. However, by comparing Figs. 10–12, it can be found that the SL, the simplified Lorentz linearization and the Lorentz linearization approaches show

Table 4
Comparison of computational efficiency of different dynamic modeling approaches in SC 3.

Numerical approach	Computational time
Lorentz linearization method	1.6×10^{-2} s
Simplified Lorentz linearization method	6.6×10^{-3} s
SL method	7.1×10^{-3} s
TD modeling	5.1 s (single-run)

a tendency to deviate more from the nonlinear TD model with the increase of the wave steepness. Moreover, it can be seen that the SL approach predicts closer pressure results to those of the nonlinear TD model than the simplified Lorentz linearization and the Lorentz linearization approach in rather high wave steepness.

The time series of the regenerated pressure results at one specific point on the floater hull are further analyzed, and the location of the examined point is illustrated in Fig. 13. Fig. 14 presents the time-dependent results of total hydrodynamic pressure on the floater. In SC 1 with low wave steepness, the nonlinearity of the system is insignificant. In this sense, the results of total pressure regenerated by different modeling approaches are mostly aligned with each other at the examined point. However, the deviation of regenerated pressure results by the simplified Lorentz linearization, the Lorentz linearization and the SL approaches from those by the TD model increases in SC 3 compared to that in SC 1 and SC 2. This can be explained by the comparison of the predicted global dynamic responses, as shown in Fig. 8, in which the difference of the four dynamic modeling approaches in the prediction of global dynamic responses increases with the increased wave steepness. This highlights that the discrepancy of modeling approaches in predicting global dynamic responses effectively propagates to the hydrodynamic pressure regeneration. In addition, the total pressure results regenerated by the SL approach correlate well with those of the TD model along the time while the simplified Lorentz linearization and the Lorentz linearization approaches tend to differ more from the TD model around peak pressure values. For example, in Fig. 14(c), the total pressure at approximately 215 s regenerated by the SL approach and the nonlinear TD model are 55000 and 54000 Pa while it reaches around 60000 Pa for the simplified Lorentz linearization and the Lorentz linearization approaches.

The standard deviations of the regenerated total pressure at the examined point are summarized in Table 5. Overall, when referenced against the nonlinear TD model, the SL approach consistently provides the most accurate predictions among the considered linearization methods across all simulation cases. In contrast, the simplified Lorentz linearization shows the largest deviations, while the Lorentz linearization approach demonstrates intermediate performance. It can be noted Table 5 that the relative error of the SL approach to the TD approach drops from 5.39% for SC 2 to 2.47% for SC 3 which is, however, the steepest state. Comparatively, the relative error of the SL approach in SC 3 is larger than that in SC 2 for the global response prediction, as shown in Section 3.2. This can be explained as follows. The total pressure is a sum of multiple pressure components reconstructed with harmonic elements. The prediction deviation in the phase shifts and amplitudes could result in instantaneous local discrepancies which cannot be reflected in the form of standard deviation of total pressure. For instance, in Fig. 14(c), the pressure predicted by the TD approach is closer than the SL approach to the mean value at 145 s, while it is farther than the SL approach at 200 s. To illustrate the instantaneous agreement of the modeling approaches in pressure prediction, the mean average percentage error (MAPE) of across time instants is also given in Table 6, from which a clear trend can be noted that the MAPE values of different modeling approaches increase with the wave steepness.

For the relatively mild sea state (SC 1), all linearized approaches yield reasonably close agreement with the TD results. The Lorentz

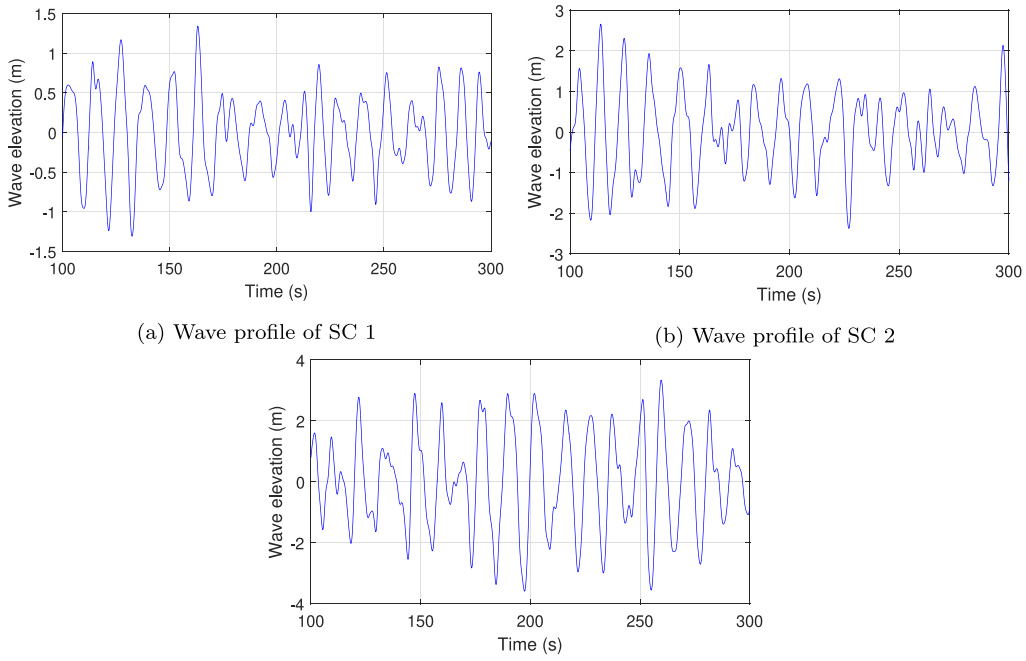

(a) Wave profile of SC 1

(b) Wave profile of SC 2

(c) Wave profile of SC 3

Fig. 7. Profiles of wave trains used for simulation cases.

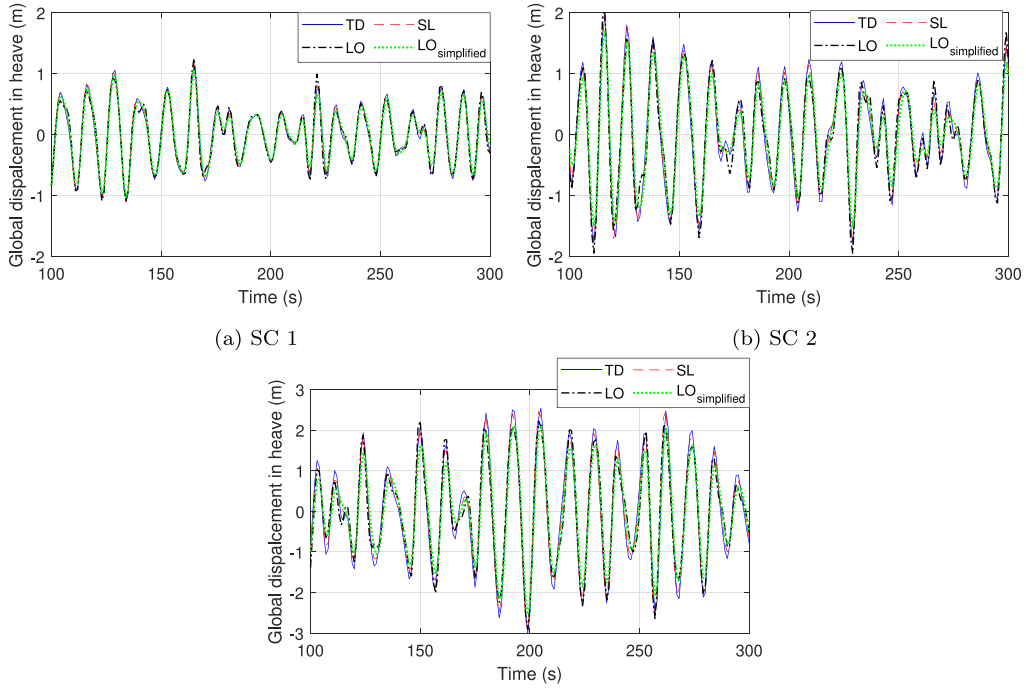

(a) SC 1

(b) SC 2

(c) SC 3

Fig. 8. Global heave displacement predicted by the four dynamic modeling approaches. Results of the simplified Lorentz linearization, Lorentz linearization and the SL approaches are obtained by IFFT.

linearization and the SL approaches produce similar relative errors of 5.16% and 4.90%, respectively, whereas the simplified Lorentz linearization method already exhibits a noticeably higher deviation of 10.39%. As the wave steepness increases in SC 2, the differences between the dynamic modeling approaches become more pronounced. The SL approach maintains adequate accuracy with a relative error of 5.39%, outperforming the Lorentz linearization approach with a relative error of 7.31%. In contrast, the simplified Lorentz linearization approach shows a significant deterioration in prediction performance,

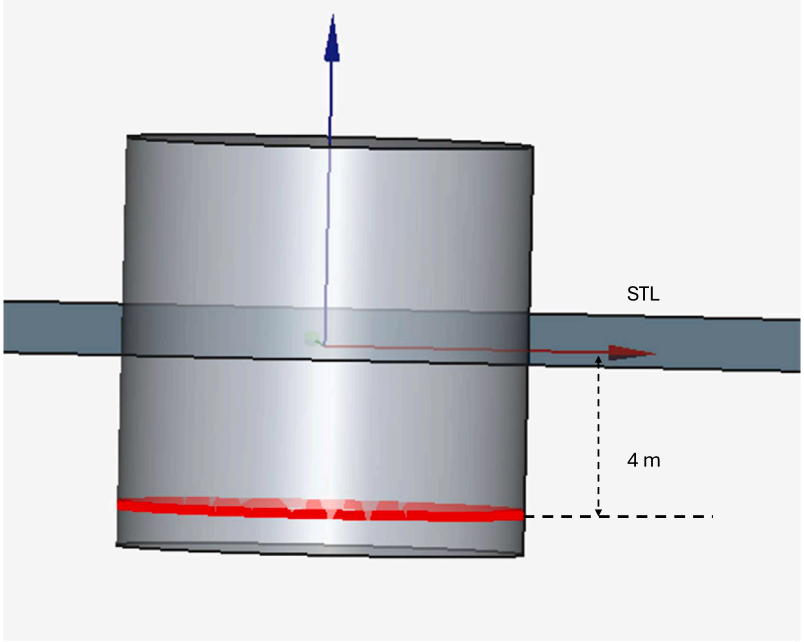

Fig. 9. Illustration of the examined cross-sectional curve of the floater.

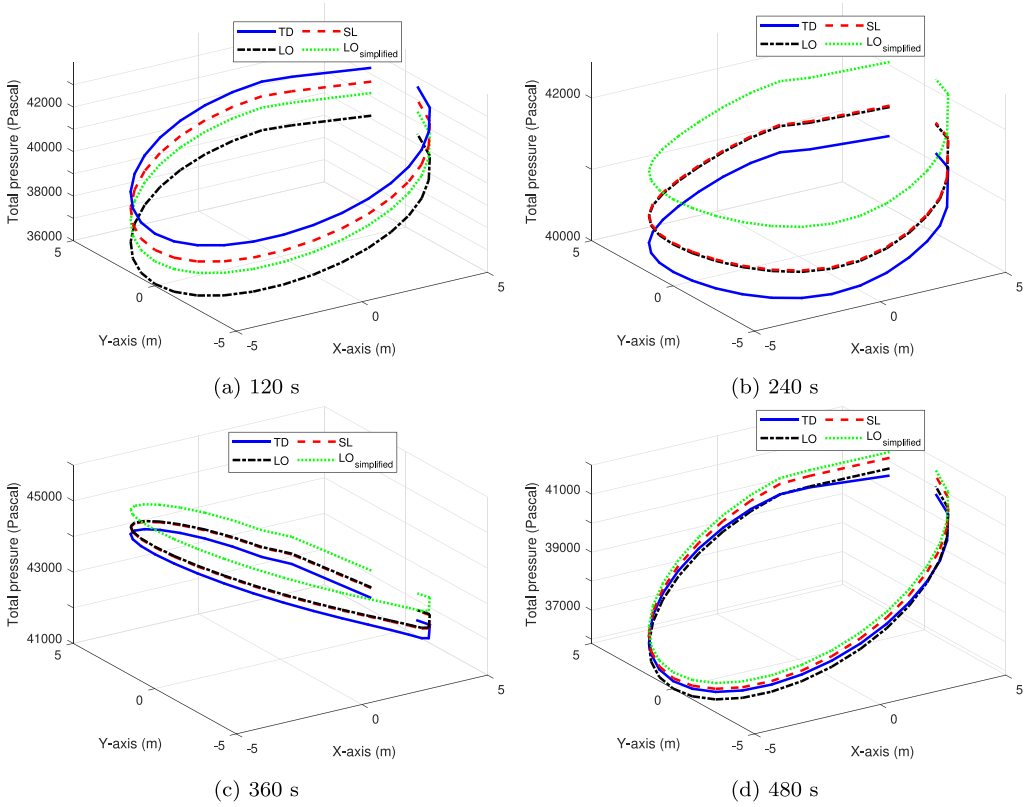

Fig. 10. Total pressure results for SC 1 along the examined curve, obtained using different dynamic models. Results are shown for four time instants.

with the relative error increasing sharply to 22.06%. This trend becomes even more evident in the steepest sea state, namely SC 3. The SL approach achieves the closest agreement with the TD model, with a relative error of only 2.47%. The Lorentz linearization exhibits a considerably larger deviation of 13.57%, while the simplified Lorentz linearization approach performs the worst, with a relative error reaching 26.98%. These results highlight that the SL approach is more robust under increasing nonlinearity, whereas the simplified Lorentz linearization fails to maintain accuracy as wave steepness increases.

The above observations further indicate that accurate prediction of global dynamic responses alone does not necessarily guarantee equally accurate regeneration of local hydrodynamic pressure. Since the pressure reconstruction procedure depends not only on the response amplitudes but also on the phase relationships between the wave excitation,

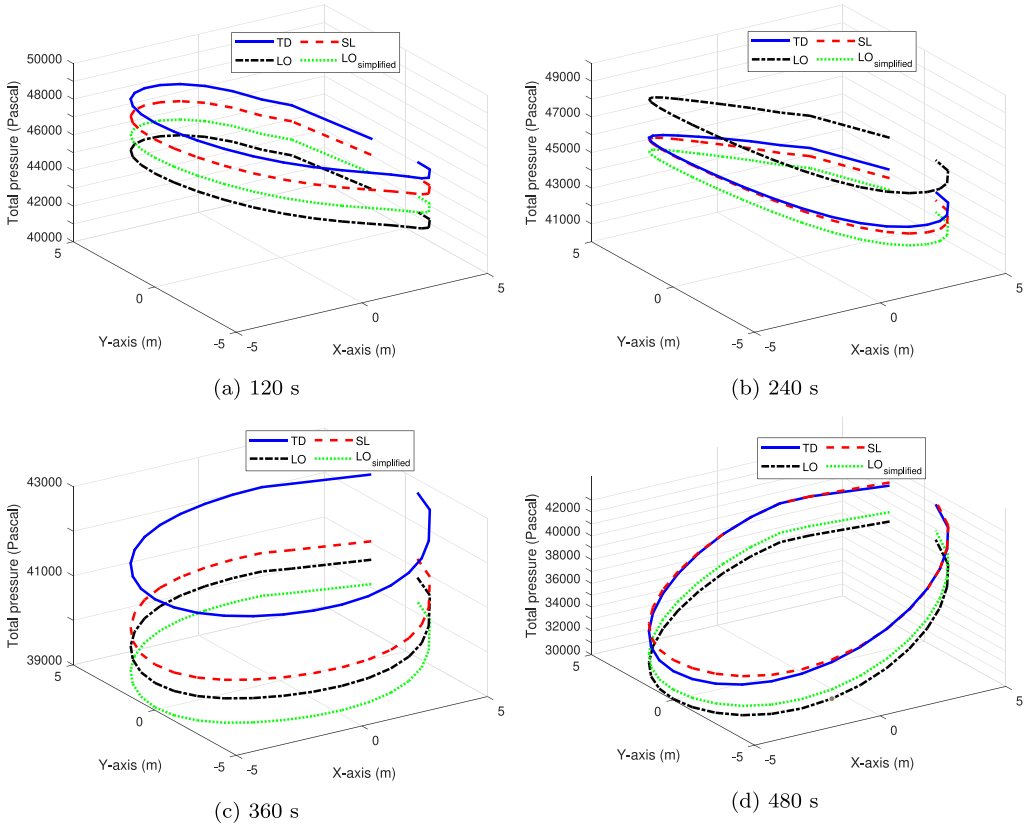

(a) 120 s (b) 240 s

(c) 360 s (d) 480 s

Fig. 11. Total pressure results for SC 2 along the examined curve, obtained using different dynamic models. Results are shown for four time instants.

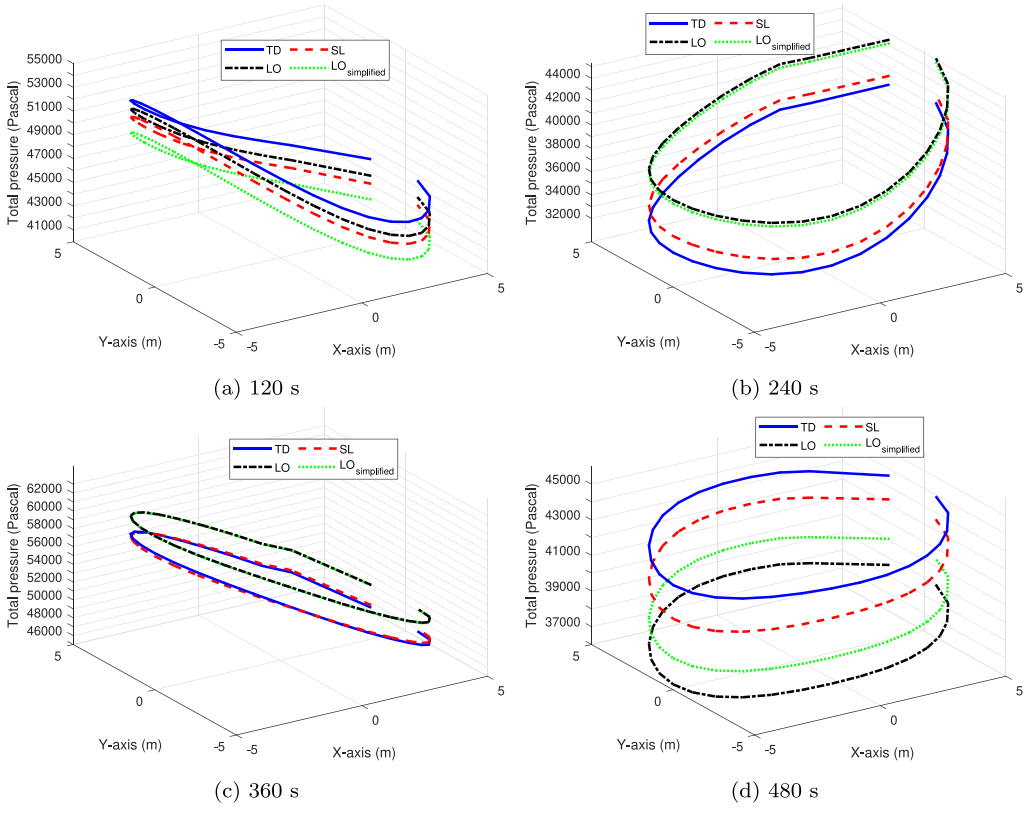

(a) 120 s (b) 240 s

(c) 360 s (d) 480 s

Fig. 12. Total pressure results for SC 3 along the examined curve, obtained using different dynamic models. Results are shown for four time instants.

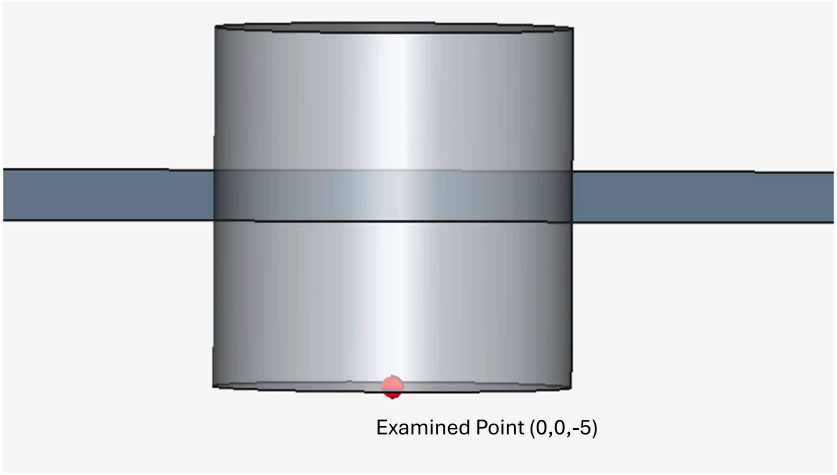

Fig. 13. Illustration of the location of the examined point at the hull of the floater.

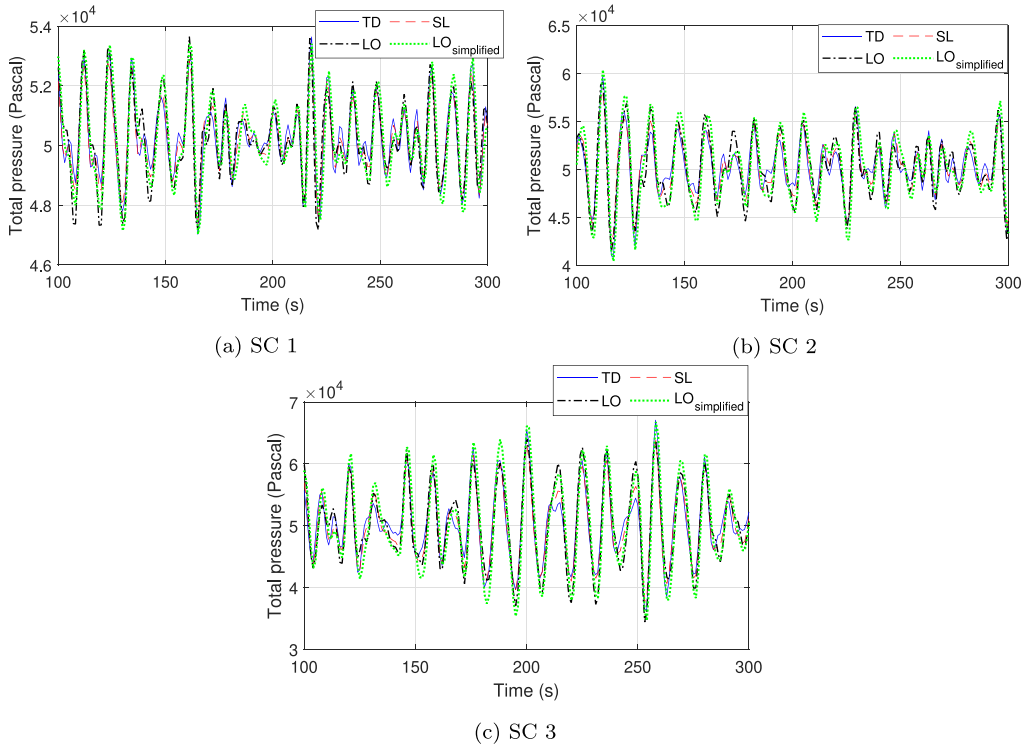

Fig. 14. Time series of total pressure at the examined point.

radiation effects, and body motions, even relatively small discrepancies in the predicted motion phase can propagate into noticeable local pressure deviations. This effect becomes increasingly significant under steeper wave conditions, where nonlinear contributions are amplified near the dominant wave frequency. In this respect, the SL approach demonstrates superior robustness because its equivalent linearization preserves the overall nonlinear energy dissipation more consistently across the frequency range, leading to improved agreement with the TD model in both global response prediction and local pressure reconstruction. In contrast, the simplified Lorentz linearization approach employs a single equivalent damping coefficient determined at the peak frequency, which tends to overestimate damping away from the spectral peak and consequently introduces larger discrepancies in both motion phasing and regenerated pressure. These findings suggest that the selection of dynamic modeling approaches can significantly influence not only global motion estimation, but also the reliability of subsequent structural loading assessments based on regenerated hydrodynamic pressure fields.

4. Discussion

While the present study provides a systematic comparison of three linearization approaches and a nonlinear TD model for predicting the hydrodynamic pressure distribution on a floating cylindrical structure, several limitations should be acknowledged to properly contextualize the findings and guide future research.

The nonlinear TD model based on the Cummins equation is adopted as the reference solution throughout this study. Although this model incorporates nonlinear external damping and is widely accepted as the standard engineering benchmark for this class of problems, it remains a model of finite fidelity. In particular, it relies on linear potential flow

Table 5
Comparison between different dynamic models on the estimation of standard deviation (STD) of total pressure at the examined point.

Case	Models	STD of pressure (Pa)	Relative error to TD (%)
SC 1	LO	1282.3	5.16
	$LO_{simplified}$	1346.1	10.39
	SL	1279.2	4.90
	TD	1219.4	–
SC 2	LO	3011.3	7.31
	$LO_{simplified}$	3425.2	22.06
	SL	2655.0	5.39
	TD	2806.1	–
SC 3	LO	6064.9	13.57
	$LO_{simplified}$	6781.1	26.98
	SL	5208.2	2.47
	TD	5340.4	–

Table 6
Comparison between mean average percentage error (MAPE) of different dynamic models with regard to the TD model on the estimation of instant total pressure at the examined point.

Case	Models	MAPE (%)
SC 1	LO	0.80
	$LO_{simplified}$	0.94
	SL	0.45
SC 2	LO	1.99
	$LO_{simplified}$	2.64
	SL	1.17
SC 3	LO	3.88
	$LO_{simplified}$	4.82
	SL	1.74

theory for the hydrodynamic coefficients and applies the mean wetted surface assumption, which introduces approximations that become less accurate under high wave steepness conditions (Palm et al., 2018). Validation against higher-fidelity references, such as fully nonlinear CFD simulations or physical model experiments, is highly recommended in future work to further establish the absolute accuracy of the TD model and, by extension, the benchmark basis of the present comparison.

In this study, the quadratic damping is selected as a representative nonlinear effect, representing a nonlinear external machinery force, to demonstrate and compare the performance of the linearization approaches. However, the SL method, by virtue of its theoretical generality, is capable of handling a broader range of nonlinear mechanisms, including nonlinear mooring forces, and force saturation arising in WECs or FOWTs (Tan et al., 2025b; Silva et al., 2021). The relative performance of the SL approach with respect to the Lorentz-based linearization methods under these alternative nonlinearity types has not been examined in the present study, and remains an important direction for future investigation.

The primary focus of the present study is to compare different dynamic modeling approaches in terms of their accuracy in predicting dynamic responses under irregular sea states, and to examine how the resulting deviations propagate to the hydrodynamic pressure distribution. In this context, it is noted that the linearization procedure for the considered nonlinearity, namely the quadratic external damping, operates on the equation of motion and remains fundamentally the same regardless of whether a single-DOF or a multi-DOF system is considered. Extending to multiple degrees of freedom would more realistically represent the dynamics of a floating structure, but would not alter the theoretical basis or the relative performance of the linearization approaches with respect to the nonlinear TD model for this particular type of nonlinearity. In order to provide a clean and well-controlled comparison that isolates the effect of the dynamic modeling choice from the additional complexity introduced by cross-coupling between DOFs, the present study is restricted to the heave degree of freedom of a cylindrical floater under the considered wave conditions. The extension of the present comparative framework to multi-DOF motion, particularly for non-axisymmetric geometries would inevitably more realistically reveal the performance of these modeling approaches on pressure reconstruction, which remains an important direction for future work.

The floating structure considered in this study is a vertical cylinder with a uniform circular cross-section, which represents a simple but commonly-encountered geometry in offshore engineering practice. This choice is deliberate, as the cylindrical geometry yields well-defined hydrodynamic characteristics and allows the comparison between modeling approaches to be conducted without interference from geometry-induced complexities. However, realistic floating offshore structures, such as semi-submersible platforms, spar buoys, or ship-shaped hulls, feature more complex geometries that might give rise to stronger nonlinear hydrodynamic effects, more intricate pressure distributions over the wetted surface, and potentially larger deviations between different modeling approaches. The extent to which the conclusions of the present study generalize to such geometries remains to be examined, and constitutes a meaningful extension of this work. In addition, the mooring system is modeled as a linear spring with stiffness, providing a light restoring force in the heave direction. This simplified representation neglects the nonlinear geometric and material stiffness characteristics of realistic catenary or taut mooring systems, as well as the associated viscous drag and inertia of mooring lines (Davidson and Ringwood, 2017). Under large amplitude motions or in extreme sea states, the nonlinear mooring restoring force can significantly contribute to the global dynamics of the floater and thereby affects the relative accuracy of these modeling approaches. The effect of a more realistic nonlinear mooring model on the comparative conclusions of this study represents meaningful future investigation.

Finally, in this study, the BEM solver NEMOH is used to compute the global hydrodynamic coefficients and the frequency-dependent diffraction and radiation pressure components distributed over the wetted surface panels. The accuracy of the predicted pressure distribution is therefore directly dependent on the fidelity of the BEM solution, including the panel mesh resolution, frequency increment, and the numerical integration scheme employed. Differences between common BEM solvers, such as NEMOH, WAMIT, ANSYS AQWA (Penalba et al., 2017b; Mazarakos, 2025), in the computation of these frequency-dependent pressure transfer functions may introduce non-negligible discrepancies in the regenerated pressure field, independent of the choice of dynamic modeling approach. This source of uncertainty has not been addressed in the present study, and a systematic assessment of BEM solver sensitivity on the pressure regeneration results is recommended for future work.

5. Conclusion

This study compares four dynamic modeling approaches, namely nonlinear TD modeling, Lorentz linearization, simplified Lorentz linearization, and the SL approach, for predicting the dynamic responses and the hydrodynamic pressure distribution of floating structures. Adopting a generic heaving cylindrical floater, the dynamic modeling approaches are first employed to predict the global dynamic responses of the floater, based on which the hydrodynamic pressure components are reconstructed using linear potential flow theory. A representative nonlinear effect, describing nonlinear external machinery forces, is incorporated in the nonlinear TD model as well as in the Lorentz linearization, simplified Lorentz linearization, and SL approaches. The TD model is formulated based on the Cummins equation with a time-dependent function representing the nonlinear effect, whereas the other approaches rely on different linearized representations of the nonlinearity.

The results demonstrate that the selection of dynamic modeling approaches has a noticeable influence on the predicted global dynamic responses, particularly as wave steepness increases. While all approaches yield similar predictions under low wave steepness conditions, clear differences emerge for more energetic sea states. The SL approach consistently shows the closest agreement with the nonlinear TD model in the prediction of global dynamic responses across all examined cases. In contrast, both the Lorentz linearization and the simplified Lorentz linearization approaches exhibit increasing deviations near the peak frequency range, where nonlinear effects are most pronounced. Moreover, the simplified Lorentz linearization tends to underestimate high-frequency responses due to the use of a single equivalent damping term derived at the peak frequency. These differences in linearization strategies result in distinct equivalent damping coefficients, which inherently lead to discrepancies in both PSD values and phase shifts compared to the nonlinear TD model.

Discrepancies in global response predictions are reflected in deviations in the reconstructed pressure distributions. Considering the examined simulation cases, at a representative point on the wetted surface, the standard deviation of the total pressure predicted using the simplified Lorentz linearization reaches relative errors up to 26.98% in the most severe sea state (SC 3), while the Lorentz linearization approach shows intermediate deviations with errors up to 13.57%. In comparison, the SL approach maintains substantially lower relative errors, down to 2.47% for the same case. Meanwhile, all linearized approaches offer substantial computational advantages, with the SL and simplified Lorentz linearization approaches achieving more than a 700-fold reduction, and the Lorentz linearization approach about a 300-fold reduction in computational cost compared to a single run of TD modeling simulation. Overall, the findings underline the strong potential of the SL approach as an accurate and efficient alternative for hydrodynamic pressure regeneration of floating structures, while indicating that the simplified Lorentz linearization and Lorentz linearization should be applied with caution in random sea states with rather high wave steepness.

CRediT authorship contribution statement

Jian Tan: Writing – review & editing, Writing – original draft, Visualization, Validation, Supervision, Software, Resources, Methodology, Investigation, Funding acquisition, Formal analysis, Data curation, Conceptualization. **George Lavidas:** Writing – review & editing, Supervision, Project administration, Methodology, Investigation, Funding acquisition, Formal analysis, Conceptualization. **Harry Bradford Bingham:** Writing – review & editing, Writing – original draft, Visualization, Validation, Supervision, Resources, Methodology, Investigation, Formal analysis, Conceptualization.

Declaration of competing interest

The authors declare that they have no known competing financial interests or personal relationships that could have appeared to influence the work reported in this paper.

Acknowledgments

H.B. Bingham appreciates the support from the Dept. of Civil and Mechanical Engineering, DTU.

G. Lavidas and J. Tan gratefully acknowledge the financial support of the Dutch Research Council (Nederlandse Organisatie voor Wetenschappelijk Onderzoek, NWO; Grant No. EP.1602.22.001) and the CETPartnership Netherlands through the Clean Energy Transition Partnership (CETPartnership) 2022 Joint Call for Research Proposals. This project was co-funded by the European Commission under Grant Agreement No. 101069750 and supported through Project No. CETP-2022-00127.

Appendix. Mathematical derivation of statistical linearization

The primary derivation process of statistical linearization is presented here, and more details can be found in Roberts and Spanos (2003). For a nonlinear function F_{non}, expressed as

$$F_{non} = f(u), \tag{A.1}$$

where u stands for a zero-mean random variable and $f(u)$ represents a mathematical formula with respect to u. Let its linear approximation function, denoted as $f_{eq}(u)$, be expressed as

$$f_{eq}(u) = Nu + Q. \tag{A.2}$$

Here, N embodies the equivalent linearized representation, which can be $R_{eq,vis}$, $K_{eq,ext}$ or $R_{eq,ext}$ in (5) and Q is the mean part of the nonlinear function f_u. The error introduced by the linearization is then calculated as

$$\epsilon = f(u) - Nu - Q. \tag{A.3}$$

For a stochastic process, the expected value of the error squared, namely $\mathbf{E}\left[\epsilon^2\right]$, can be derived as

$$\mathbf{E}\left(\epsilon^2\right) = \mathbf{E}\left[(f(u) - Nu - Q)^2\right], \tag{A.4}$$

where $\mathbf{E}(\cdot)$ represents the expected value of a function. Minimizing the squared error requires N and Q to satisfy the following conditions:

$$\frac{\mathrm{d}}{\mathrm{d}N}\mathbf{E}\left(\epsilon^2\right) = 0 \quad \text{and} \quad \frac{\mathrm{d}}{\mathrm{d}Q}\mathbf{E}\left(\epsilon^2\right) = 0. \tag{A.5}$$

This leads to

$$N = \frac{\mathbf{E}\left[uf(u)\right]}{\mathbf{E}\left(u^2\right)} = \frac{\mathbf{E}\left[uf(u)\right]}{\sigma_u^2}, \tag{A.6}$$

where the expected value of the numerator can be calculated as

$$\mathbf{E}\left[uf(u)\right] = \int_{-\infty}^{\infty} uf(u)p(u)\mathrm{d}u, \tag{A.7}$$

where σ_u is the standard deviation of the variable u; $p(u)$ is the probability density function of the variable u. Assuming that the variable u follows a Gaussian distribution, the probability density function is then expressed as

$$p(u) = \frac{1}{\sigma_u\sqrt{2\pi}}\exp(-\frac{u^2}{2\sigma_u^2}). \tag{A.8}$$

Applying (A.6) to the functions (4) gives the equivalent linearized coefficient of the considered nonlinearity in this work.

Acronyms

Acronym	Description
BEM	Boundary Element Method
CFD	Computational Fluid Dynamics
DNV	Det Norske Veritas
FD	Frequency Domain
FEM	Finite Element Method
FOWT	Floating Offshore Wind Turbine
FFT	Fast Fourier Transform
IFFT	Inverse Fast Fourier Transform
RAO	Response Amplitude Operator
SL	Statistical Linearization
TD	Time Domain
WEC	Wave Energy Converter

Symbols

Symbol	Description
ω_j	Angular frequency of jth wave component
ω_p	Peak angular frequency
ϕ_j	Random phase angle of jth wave component
A_j	Wave amplitude of jth wave component
A_{lo}	Localized wave amplitude
k_j	Wave number of jth wave component
$S(\omega_j)$	Wave spectral density
N	Number of wave components
t	Time
$\delta(\cdot)$	Dirac delta function
$\Delta\omega$	Frequency interval
ϵ	Wave steepness
λ	Wavelength
M	Mass of floating structure
M_{cy}	Mass of cylindrical floater
$M_r(\infty)$	Added mass at infinite frequency
z	Displacement
$\dot{z}$	Velocity
$\ddot{z}$	Acceleration
F_e	Wave excitation force
$\hat{F}_e$	Complex amplitude of excitation force
$\hat{f}_e$	Excitation force coefficient
$F_{mooring}$	Mooring restoring force
F_{hs}	Hydrostatic restoring force
F_{ext}	Nonlinear external damping force
K_{hs}	Hydrostatic stiffness coefficient
$K_{mooring}$	Mooring stiffness coefficient
K_{rad}	Radiation impulse response function
R_r	Radiation damping coefficient
R_{ext}	External damping coefficient
$R_{SL,ext}$	Statistical linearization damping coefficient
$R_{LO,ext}$	Lorentz linearization damping coefficient
$P_{i,j}^{\text{diff}}$	Diffraction pressure amplitude at point i for jth wave component
$\phi_{i,j}^{\text{diff}}$	Diffraction pressure phase angle at point i for jth wave component
$P_{i,m,j}^{\text{rad}}$	Radiation pressure amplitude at point i for mth DOF and jth frequency component
$\phi_{i,m,j}^{\text{rad}}$	Radiation pressure phase angle at point i for mth DOF and jth frequency component
$p_i^{\text{FK}}(t)$	Froude–Krylov pressure at point i
$p_i^{\text{diff}}(t)$	Diffraction pressure at point i
$p_i^{\text{hs}}(t)$	Hydrostatic pressure at point i
$p_i^{\text{rad}}(t)$	Radiation pressure at point i
$p_i^{\text{total}}(t)$	Total pressure at point i on hull surface
$\mathbf{Z}(t)$	Time-domain motion vector of floater
$\hat{\mathbf{u}}_{m,j}$	Complex velocity amplitude of floater in mth DOF at frequency ω_j
ρ	Water density
g	Gravitational acceleration
$\mathbf{n}$	Unit normal vector
τ	Convolution variable
$\hat{z}$	Complex amplitude of displacement
$\hat{z}_{lo}$	Complex amplitude of displacement using Lorentz linearization method

References

2016. Numerical Modelling of Wave Energy Converters. Numerical Modelling of Wave Energy Converters. ISBN: 9780128032107, http://dx.doi.org/10.1016/c2014-0-04006-3.

Abdelmoteleb, S.-E., Bachynski-Polić, E.E., 2025. A frequency-domain optimization procedure for catenary and semi-taut mooring systems of floating wind turbines. Mar. Struct. 101, 103768.

Al Shami, E., Wang, X., Zhang, R., Zuo, L., 2019. A parameter study and optimization of two body wave energy converters. Renew. Energy 131, 1–13.

Chakrabarti, S., 1998. Physical model testing of floating offshore structures. In: Dynamic Positioning Conference, vol. 1, Offshore Structure Analysis, Inc, pp. 1–33.

Cummins, W., Iiuhl, W., Uinm, A., 1962. The impulse response function and ship motions.

Davidson, J., Ringwood, J.V., 2017. Mathematical modelling of mooring systems for wave energy converters - A review. Energies (ISSN: 19961073) 10 (5), http://dx.doi.org/10.3390/en10050666.

DNV, G., 2019. SESAM user manual, WADAM, wave analysis by diffraction and morison theory. HøVik, Nor..

Folley, M., Whittaker, T., 2010. Spectral modelling of wave energy converters. Coast. Eng. 57 (10), 892–897.

Folley, M., Whittaker, T., 2013. Validating a spectral-domain model of an OWC using physical model data. Int. J. Mar. Energy 2, 1–11.

Gao, Z., Merino, D., Han, K.-J., Li, H., Fiskvik, S., 2023. Time-domain floater stress analysis for a floating wind turbine. J. Ocean. Eng. Sci. 8 (4), 435–445.

Hall, M.T.J., 2013. Mooring line modelling and design optimization of floating offshore wind turbines (Ph.D. thesis).

Huo, F.-l., Luo, P., Nie, Y., Zhao, Y.-p., Li, M.-y., Xu, S., 2024. Structural strength study of a floating wind turbine under freak waves through the CFD-fea method. China Ocean Eng. 38 (6), 943–957.

Jonkman, J.M., 2009. Dynamics of offshore floating wind turbines—model development and verification. Wind. Energy: An Int. J. Prog. Appl. Wind. Power Convers. Technol. 12 (5), 459–492.

Journée, J.M.J., Massie, W.W., Huijsmans, R.H.M., 2015. Offshore hydrodynamics.

Karimirad, M., 2014. Offshore Energy Structures: for Wind Power, Wave Energy and Hybrid Marine Platforms. Springer.

Kluger, J.M., Sapsis, T.P., Slocum, A.H., 2016. A reduced-order, statistical linearization approach for estimating nonlinear floating wind turbine response statistics. In: ISOPE International Ocean and Polar Engineering Conference. ISOPE, pp. ISOPE–I.

Kvittem, M.I., Moan, T., 2015. Time domain analysis procedures for fatigue assessment of a semi-submersible wind turbine. Mar. Struct. 40, 38–59.

Lawson, M., Yu, Y.-H., Ruehl, K., Michelen, C., et al., 2014. Development and demonstration of the WEC-sim wave energy converter simulation tool.

Luan, C., Gao, Z., Moan, T., 2017. Development and verification of a time-domain approach for determining forces and moments in structural components of floaters with an application to floating wind turbines. Mar. Struct. 51, 87–109.

Magagna, D., Uihlein, A., 2015. Ocean energy development in europe: Current status and future perspectives. Int. J. Mar. Energy 11, 84–104.

Martínez, M.L., Chávez, V., De la Cruz, V., Pérez-Maqueo, O., Wojtarowski, A., Silva, R., 2023. Ocean energy. In: The Palgrave Handbook of Global Sustainability. Springer, pp. 177–192.

Mazarakos, T., 2025. Comparison of second-order wave loads on a floating cylinder wec between NEMOH and ANSYS AQWA. In: Innovations in the Analysis and Design of Marine Structures. CRC Press, pp. 3–11.

Palm, J., Eskilsson, C., Bergdahl, L., Bensow, R., 2018. Assessment of Scale Effects, Viscous Forces and Induced Drag on a Point-Absorbing Wave Energy Converter by CFD Simulations. J. Mar. Sci. Eng. 6 (4), 124. http://dx.doi.org/10.3390/jmse6040124.

Penalba, M., Kelly, T., Ringwood, J., 2017a. Using NEMOH for Modelling Wave Energy Converters : A Comparative Study with WAMIT. In: 12th European Wave and Tidal Energy Conference. p. 10.

Penalba, M., Kelly, T., Ringwood, J., 2017b. Using NEMOH for modelling wave energy converters: A comparative study with WAMIT.

Pérez, T., Fossen, T., 2008. Time-vs. frequency-domain identification of parametric radiation force models for marine structures at zero speed. Model. Identif. Control 29 (1), 1–19.

Roberts, J.B., Spanos, P.D., 2003. Random Vibration and Statistical Linearization. Courier Corporation.

Robertson, A., Jonkman, J., Musial, W., Vorpahl, F., Popko, W., 2013. Offshore Code Comparison Collaboration, Continuation: Phase II Results of a Floating Semisubmersible Wind System. Technical Report, National Renewable Energy Lab.(NREL), Golden, CO (United States).

Shi, H., Huang, S., Cao, F., 2019. Hydrodynamic performance and power absorption of a multi-freedom buoy wave energy device. Ocean Eng. 172, 541–549.

Silva, L., Cazzolato, B., Sergiienko, N., Ding, B., 2021. Nonlinear dynamics of a floating offshore wind turbine platform via statistical quadratization—Mooring, wave and current interaction. Ocean Eng. 236, 109471.

Silva, L., Sergiienko, N., Pesce, C., Ding, B., Cazzolato, B., Morishita, H., 2020. Stochastic analysis of nonlinear wave energy converters via statistical linearization. Appl. Ocean Res. 95, 102023.

Suzuki, H., Shiohara, H., Schnepf, A., Houtani, H., Carmo, L.H., Hirabayashi, S., Haneda, K., Chujo, T., Nihei, Y., Malta, E.B., et al., 2020. Wave and wind responses of a very-light fowt with guy-wired-supported tower: Numerical and experimental studies. J. Mar. Sci. Eng. 8 (11), 841.

Tan, J., Coe, R.G., Lavidas, G., 2025a. Benchmark of numerical modeling approaches on the systematic performance evaluation of wave energy converters. Appl. Ocean Res. 162, 104725.

Tan, J., Polinder, H., Laguna, A.J., Miedema, S., 2022a. The application of the spectral domain modeling to the power take-off sizing of heaving wave energy converters. Appl. Ocean Res. 122, 103110.

Tan, J., Polinder, H., Laguna, A.J., Miedema, S., 2022b. A numerical study on the performance of the point absorber wave energy converter integrated with an adjustable draft system. Ocean Eng. 254, 111347.

Tan, J., Polinder, H., Laguna, A.J., Miedema, S., 2023a. A wave-to-wire analysis of the adjustable draft point absorber wave energy converter coupled with a linear permanent-magnet generator. Ocean Eng. 276, 114195.

Tan, J., Tao, W., Laguna, A.J., Polinder, H., Xing, Y., Miedema, S., 2023b. A spectral-domain wave-to-wire model of wave energy converters. Appl. Ocean Res. 138, 103650.

Tan, J., Zuo, L., Lavidas, G., Metrikine, A., 2025b. Extending the statistical linearization method to multi-variate non-differentiable nonlinearities in floating renewable energy devices. Renew. Energy 123964.

Terra, G.M., van de Berg, W.J., Maas, L.R., 2005. Experimental verification of Lorentz'linearization procedure for quadratic friction. Fluid Dyn. Res. 36 (3), 175.

Tom, N., Lawson, M., Yu, Y.-H., Wright, A., 2016. Development of a nearshore oscillating surge wave energy converter with variable geometry. Renew. Energy 96, 410–424.

Wang, S., Moan, T., Gao, Z., 2023. Methodology for global structural load effect analysis of the semi-submersible hull of floating wind turbines under still water, wind, and wave loads. Mar. Struct. 91, 103463.

Xu, Q., Li, Y., Yu, Y.-H., Ding, B., Jiang, Z., Lin, Z., Cazzolato, B., 2019. Experimental and numerical investigations of a two-body floating-point absorber wave energy converter in regular waves. J. Fluids Struct. 91, 102613.